A Silicon Integrated Micro Positioning *xy*-Stage for Nano-Manipulation*

Wang Jiachou[1,†], Rong Weibin[1], Sun Lining[1], and Li Xinxin[2]

(1 *State Key Laboratory of Robotics and System, Harbin Institute of Technology, Harbin* 150001, *China*)
(2 *State Key Laboratory of Transducer Technology, Shanghai Institute of Microsystem and Information Technology, Chinese Academy of Sciences, Shanghai* 200050, *China*)

Abstract: An integrated micro positioning *xy*-stage with a 2mm×2mm-area shuttle is fabricated for application in nanometer-scale operation and nanometric positioning precision. It is mainly composed of a silicon-based *xy*-stage, electrostatics comb actuator, and a displacement sensor based on a vertical sidewall surface piezoresistor. They are all in a monolithic chip and developed using double-sided bulk-micromachining technology. The high-aspect-ratio comb-driven *xy*-stage is achieved by deep reactive ion etching (DRIE) in both sides of the wafer. The detecting piezoresistor is located at the vertical sidewall surface of the detecting beam to improve the sensitivity and displacement resolution of the piezoresistive sensors using the DRIE technology combined with the ion implantation technology. The experimental results verify the integrated micro positioning *xy*-stage design including the micro *xy*-stage, electrostatics comb actuator, and the vertical sidewall surface piezoresistor technique. The sensitivity of the fabricated piezoresistive sensors is better than 1.17mV/μm without amplification and the linearity is better than 0.814%. Under 30V driving voltage, a $\pm 10\mu$m single-axis displacement is measured without crosstalk and the resonant frequency is measured at 983Hz in air.

Key words: MEMS; integrated micro *xy*-stage; electrostatics comb actuator; vertical sidewall surface piezoresistor in plane
PACC: 0670D; 2940T; 2940P
CLC number: TP212 **Document code**: A **Article ID**: 0253-4177(2008)10-1932-07

1 Introduction

Micro-fabricated *xy*-stages have mainly been studied in the micro-operation region. They have had an impact, not only on the miniaturization of bulky mechanical systems, but also on the realization of high precision systems. Electrostatic actuation is a frequently used method in microelectromechanical systems (MEMS). Since demonstrated for the first time by Tang *et al*.[1], comb drive actuators, which play an important role, have been widely used in micro/nano manipulation. A two-dimensional micro *xy*-stage can be formed by combining these electrostatic comb actuators for precision positioning and micro/nano manipulation. With the capability of controllable linear displacement in the range of micrometers, by providing controlled displacement in one or two degrees-of-freedom, the micro *xy*-stage has been used in many applications[2], such as micro optical lens scanner[3~5], high-density data storage[6,7], scanning probe microscopy (SPM)[8,9], optical cross-connections[10], and bimolecular manipulation[11,12].

A single-wafer-processed nano-positioning *xy*-stage with trench-sidewall micromachining technique was fabricated by Gu *et al*.[13]. Unfortunately, these micro positioning stages mentioned above all lack of the function of displacement detection due to the limitation of the dimension of the silicon-based micro *xy*-stage to integrate the displacement sensor into the stage. So it is difficult to improve their positioning accuracy further.

In this paper, to improve positioning accuracy and nanometer-scale operation to meet special application needs, a micro nano-positioning *xy*-stage integrated with piezoresistive displacement sensors is proposed. It is improved on the basis of the micro *xy*-stage mentioned in Ref. [13] and fabricated on the single-crystal silicon (SCS) substrate of the silicon-on-glass (SOG) using anodic bonding process. Air trenches are used to isolate the different electrostatic comb actuators. Moreover, a vertical sidewall surface piezoresistive displacement sensor is integrated into the fabricated micro *xy*-stage to detect output displacement using the DRIE technology combined with the ion implantation technology. All of these, espe-

* Project supported by the National Natural Science Foundation of China (No. 50725518), the State Key Development Program for Basic Research of China (No. 2007AA04Z315), and the Program for Changjiang Scholars and Innovative Research Team in University
† Corresponding author. Email: jiatao_wang@163.com
Received 12 May 2008, revised manuscript received 19 June 2008

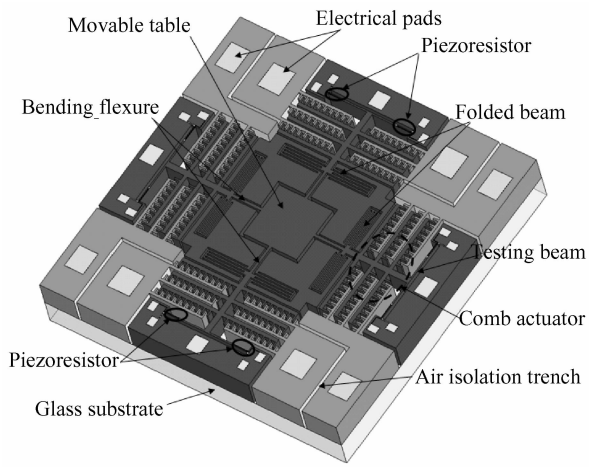

Fig. 1　Schematic of the micro *xy*-stage

cially the fabricated process chart, are different from Ref. [13]. The detail fabricated process chart is introduced and the characterization of the integrated micro *xy*-stage is given.

2　Design

Figure 1 shows a complete schematic diagram of the integrated micro nano-positioning *xy*-stage. In the kinematics mechanism design, there are four identical comb electrostatics actuators arranged perpendicular to each other, which drives in-plane movable stage in-plane movement along the axis of $+x$, $-x$, $+y$, and $-y$, respectively. Accordingly, four folded beams are used to balance the actuation force by deflection and support the movable stage and comb actuators over the substrate. The detection beam is connected to the end of the comb actuator and two piezoresistors are located at the vertical sidewall surface of the end of the detecting beam, respectively. The folded beam and bending flexure composite suspending configuration supports the movable structure over the substrate and avoids crosstalk between the movable stage movement in the *x*-direction and *y*-direction. Figure 2 shows a simplified mechanism of the proposed micro *xy*-stage.

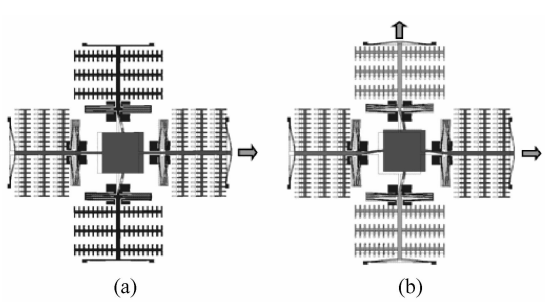

Fig. 2　Driving mechanism of the micro *xy*-stage　(a) *x*-actuation; (b) *x*- and *y*-actuation

Table 1　Detailed dimensions of the integrated micro positioning *xy*-stage

Item	Value
Number of finger pairs	2624/direction
Width of folded beam	9.5μm
Length of folded beam	1200μm
Length of bending flexure	1300μm
Width of bending flexure	9.5μm
Length of detecting beam	1200μm
Width of detecting beam	12μm
Small gap	1.7μm
Large gap	2.5μm
Structure thickness	45μm
Length of piezoresistor	300μm
Width of piezoresistor	1.6μm
Thickness of piezoresistor	4μm

Generally, a one-directional comb drive actuator has the following relationship between displacement and applied voltages:

$$y = \frac{n\varepsilon_0 h}{gk_{\text{sys}}} V^2 \tag{1}$$

where y is the static displacement, g, h, and n are the gap, thickness, and the number of comb fingers, respectively, k_{sys} is the spring stiffness of the actuator, and V is the actuated voltage. With Eq. (1) and a given actuated voltage, a large displacement can be achieved under the condition of a maximized thickness/gap aspect ratio of the comb structure and also a minimized g and k_{sys}. Table 1 shows the dimensions of the proposed *xy*-stage.

2.1　Folded-beam and bending-flexure composite suspension

The Folded beam and bending flexure composite suspension are important parts of the linear electrostatic comb actuator. Generally they are required to have large compliance in the actuation direction for possibly large displacements, and a high stiffness in the lateral direction so as to prevent side instabilities. In our design, a folded spring shown in Fig. 3 is used to support the rotor and the movable stage.

From beam deflection theory[14], the stiffness of a folded beam in the motion direction, $k_{y,\text{folded-beam}}$, and lateral direction, $k_{x,\text{folded-beam}}$, can be expressed, respectively, as:

$$k_{x,\text{folded-beam}} = 2Eh_{\text{f}}b_{\text{f}}/l_{\text{f}},\ k_{y,\text{folded-beam}} = 2Eh_{\text{f}}b_{\text{f}}^3/l_{\text{f}}^3 \tag{2}$$

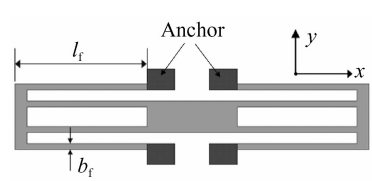

Fig. 3　Schematic of the folded beam

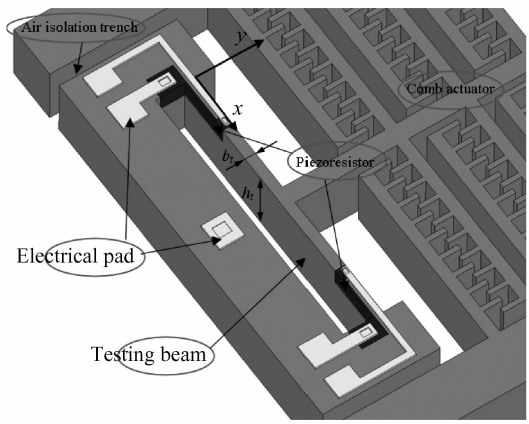

Fig. 4 3D sketch of the testing beam and piezoresistors

where E is the Young's modulus of silicon, b_f is the beam width, h_f is the thickness, and l_f is the length. Because b_f is much smaller than l_f, we get $k_{x,\text{folded-beam}} \gg k_{y,\text{folded-beam}}$. The stiffness ratio, in our design is as large as $k_{x,\text{folded-beam}}/k_{y,\text{folded-beam}} = (l_f/b_f)^2 = 1.60\times10^4$. Therefore, the designed folded flexure has a very weak cross-axis actuating influence.

The bending flexures are designed with dimensional parameters, including b_f and h_f, that are the same as those of the folded beams, except the length L. So the spring constant can be still expressed with Eq. (2) after substituting L for l_f.

$$k_{x,\text{flexure-beam}} = 2Eh_f b_f/L,\quad k_{y,\text{flexure-beam}} = 2Eh_f b_f^3/L^3 \tag{3}$$

2.2 Detecting beam and piezoresistor

Figure 4 shows a 3D schematic of the testing beam and the piezoresistors. The sensing direction of the displacement sensor is in the wafer plane. The transversely deflecting clamped-clamped beam is designed to measure the lateral displacement of the movable stage. Two piezoresistors are located at the vertical sidewall surface of both ends of the detecting beam, respectively, and two detecting beams with the identical construction are at both sides of the movable stage to form a full Wheatstone bridge (see Fig. 1). Two resistors increase their resistance, whereas, the others' resistances decrease, when the detecting beam lateral deformation occurs along the displacement of the movable stage.

Based on theoretical analysis, the deflection $w(x)$ along the lateral direction of the detecting beam can be determined as follows:

$$w(x) = \frac{F}{Eh_t b_t^3}x^2\left(\frac{3}{2}l_t - x\right) \tag{4}$$

where l_t is the length of the detecting beam, and h_t and b_t are the detecting beam height and width, respectively. The maximal deflection, $w_{\max}$, can be expressed as

$$w_{\max}(l_t) = \frac{Fl_t^3}{2Eh_t b_t^3} \tag{5}$$

According to Hook's law, the stiffness of a detecting beam in the motion direction, $k_{y,\text{testing-beam}}$, can be expressed as

$$k_{y,\text{testing-beam}} = \frac{2Eh_t b_t^3}{l_t^3} \tag{6}$$

The stress along the axial direction of the detecting beam can be obtained[15]:

$$T(x) = Eb'w''(x) = \frac{6Fb'}{h_t b_t^3}\times\left(\frac{1}{2}l_t - x\right) \tag{7}$$

where b' is the distance between the resistor and the neutral plane of the detecting beam, $0\leqslant b'\leqslant b_t/2$. So sensitivity of the sensor can be expressed as

$$\begin{aligned} V_{\text{out}} &= \frac{\pi_{44}\int_0^{l_p}T(x)\mathrm{d}x}{2l_p}V_{\text{supply}} \\ &= \frac{3\pi_{44}Fb'}{2h_t b_t^3}(l_t - l_p)V_{\text{supply}} \end{aligned} \tag{8}$$

where π_{44} is the piezoresistive coefficient, V_{supply} is the supplied voltage on the Wheatstone bridge, and l_p is the length of the piezoresistor.

2.3 Modeling of the system spring stiffness

A spring system in the x- or y-direction is composed of two pairs of folded beam spring, one pair of bending flexures, and two pairs of detecting beams. These springs are connected in parallel with each other so that the total spring stiffness in the x- or y-direction k_{sys_x}, k_{sys_y} is given, respectively, by:

$$\begin{cases} k_{\text{sys}\_x} = 2k_{x,\text{folded-beam}} + k_{x,\text{flexure-beam}} + 2k_{x,\text{testing-beam}} \\ k_{\text{sys}\_y} = 2k_{y,\text{folded-beam}} + k_{y,\text{flexure-beam}} + 2k_{y,\text{testing-beam}} \end{cases} \tag{9}$$

Therefore, the stiffness ratio of the spring system is:

$$\frac{k_{\text{sys}\_x}}{k_{\text{sys}\_y}} = \frac{2k_{x,\text{folded-beam}} + k_{x,\text{flexure-beam}} + 2k_{x,\text{testing-beam}}}{2k_{y,\text{folded-beam}} + k_{y,\text{flexure-beam}} + 2k_{y,\text{testing-beam}}} \tag{10}$$

2.4 Comb-finger electrostatic actuator design

As indicated in Eq. (1), the electrostatic actuating efficiency is defined as the moving distance as a function of the actuating voltage. In our design, in order to improve the actuating efficiency, n is chosen to be 2624. We use two-segment comb-finger configurations to further improve the actuating efficiency[13]. The two segments are connected by a line with a slope of 0.213, as shown in Fig. 5.

For this actuator design, when the displacement exceeds about 4.0μm, the comb fingers move within the small gap, 1.7μm. The displacement of the movable stage can be expressed as

$$y = \frac{n\varepsilon_0 h}{g_1 k_y}V^2,\quad 0 < y \leqslant y_1$$

$$y = \frac{n\varepsilon_0 h}{g_3 k_y}\times\left(2 - \frac{g_3}{g_1}\right)V^2,\quad y_1 < y \leqslant y_2$$

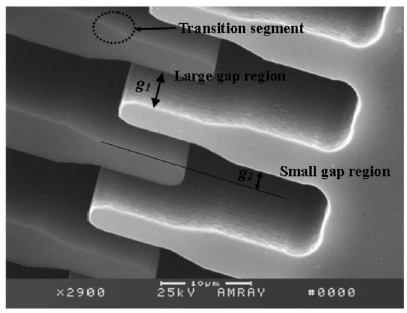

Fig. 5　SEM image of the two-segment comb-finger

$$g_3 = g_1 - 0.213(y - y_1)$$
$$y = \frac{n\varepsilon_0 h}{g_2 k_y} \times \left(2 - \frac{g_2}{g_1}\right) V^2, \quad y > y_2 \qquad (11)$$

where g_3 is in the transition region. For the displacement from the original position to y_1, the comb fingers move in the large gap region. When the displacement exceeds y_2, the comb fingers move in the small region, and, displacement from y_1 to y_2 occurs in the transition region.

3　FEA structural analysis

A finite element analysis (FEA) simulation is used to study the stiffness of the structure and to estimate the natural frequency and mode shapes of the designed system. Figure 6 shows the result of the modal analysis of the proposed *xy*-stage. It shows that the first and second modes are the result of actuation with respect to the *x*- or *y*-direction and the third mode is related to the rotation of the movable stage.

4　Fabrication

The fabrication process of the micro *xy*-stage is based on the anodic bonding process and double sided bulk-micromachining technologies in which the vertical sidewall surface piezoresistor technique plays an important role. In this process, the piezoresistive sensor is integrated in the vertical sidewall surface of the detecting beam. The process includes five patterning and two DRIE etching steps. The fabrication process for the micro stage is depicted in Fig. 7 and described as follows.

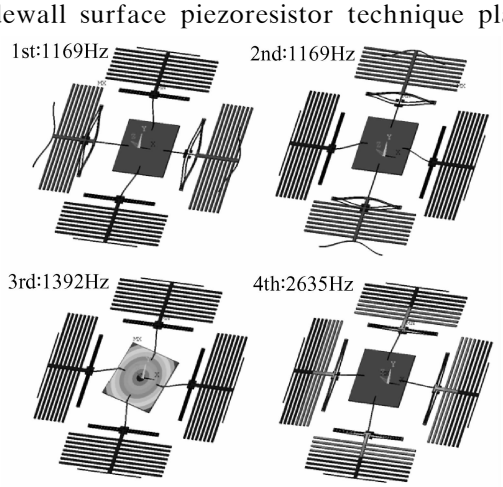

Fig. 6　Modal shapes analysis (without damping conditions)

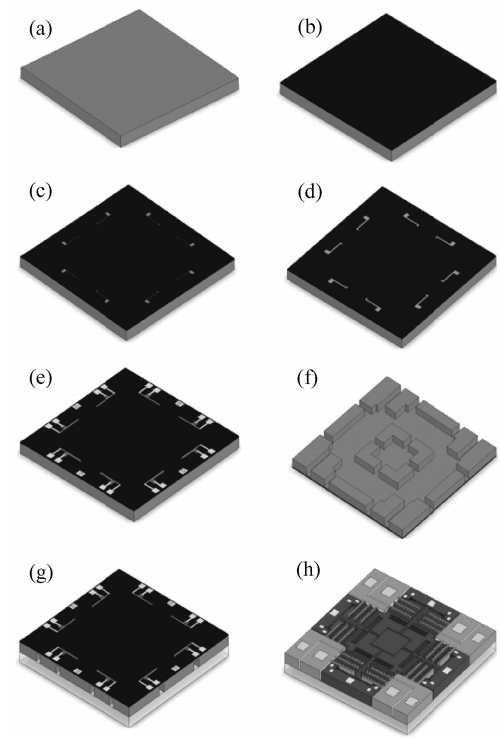

Fig. 7　Fabrication process of the micro *xy*-stage

(1) We start with double polished n-type (100)-oriented 100mm ordinary silicon wafers with a resistivity of 1～10Ω·cm;

(2) The SiO_2 layer is grown on both side of the silicon wafers by the thermal oxidation process;

(3) Photolithography is first conducted on the front side of the wafer to pattern the piezoresistors, and then buffer HF acid etching SiO_2 with photoresist as the etching mask;

(4) The wafer surface piezoresistors are formed by a boron ion implantation process. In order to form better ohmic contacts in the next step, the impurity concentration on the wafer surface is controlled at about 10^{19} atoms/cm^3;

(5) After the second photolithography step, the contact hole is formed by buffer HF acid etching, and then aluminum is sputtered and patterned for a third photolithography step. The metallization process is performed for interconnection;

(6) The backside release window is patterned in the fourth photolithography step, then the DRIE Bosch process is used to thin the device regions to 50μm with a photoresist (AZ9260) as the etching mask;

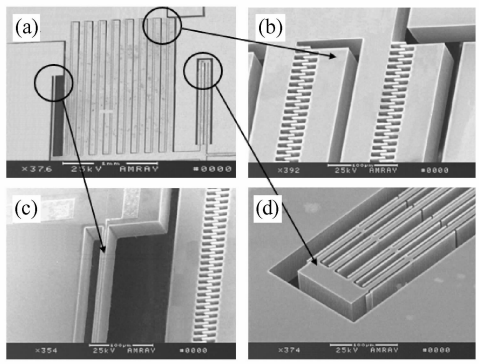

Fig. 8 SEM images showing close-up views of the *xy*-stage

(7) An anodic bonding process is used to bond glass and the backside of the silicon wafer;

(8) With a patterned photoresist and a SiO_2 layer as the etching mask, the mechanical structure and the vertical sidewall surface piezoresistors on the testing beam are synchronously formed using DRIE. In order to ensure identical dimensions for each piezoresistor, the parameters of the DRIE should be controlled strictly.

The photographs in Fig. 8 show the close-up views of the stage. Figures 9 (a) and 9 (b) show the top-view CCD micrograph of the piezoresistor. Figure 9(a) shows the wafer surface piezoresistor before forming the vertical sidewall surface piezoresistor by DRIE, and Figure 9(b) shows the fabricated vertical sidewall surface piezoresistor after being released by the DRIE. Figure 9(c) shows the SEM photo of close-up views of the end of the detecting beam, on the vertical sidewall surface of which there is a fabricated piezoresistor.

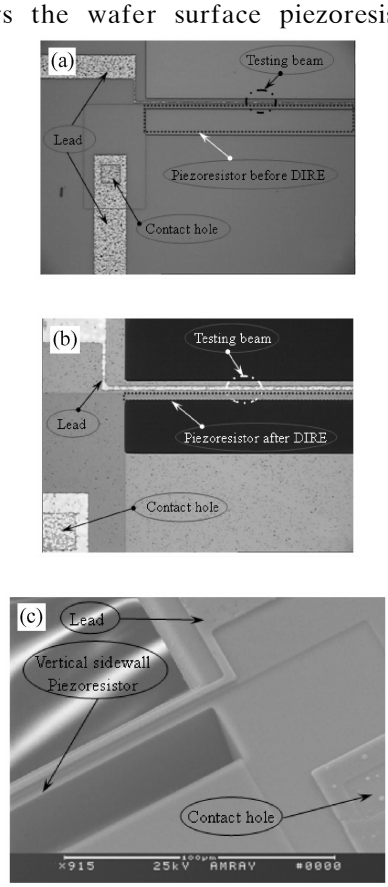

Fig. 9 (a), (b) Photograph of piezoresistor during the fabricating process; (c) Close-up view of the fabricated detecting beam and piezoresistors

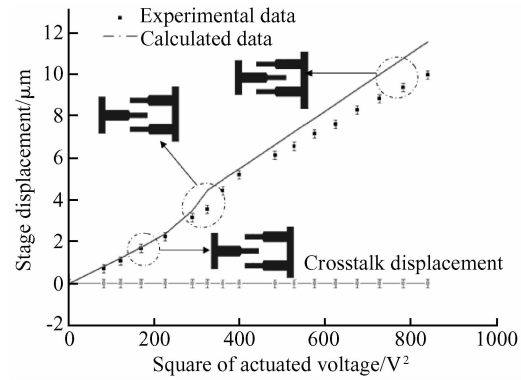

Fig. 10 Static displacement of fabricated micro *xy*-stage

5 Characterization

This section deals with characterization of the fabricated stage. The stage displacement in terms of the actuating voltage is tested by measuring the stage moving distance under a microscope scale that has a resolution of $\pm 0.1\mu$m. Figure 10 shows the static displacement of the stage at different voltages. As indicated in Fig. 10, within the resolution of the observations, no crosstalk is observed even when the maximum displacement of around 10μm is achieved for both the *x*- and *y*-axis at a driving voltage of 30V. When a single axis is fully actuated, the generated motion in the other axis is not noticeable from a high resolution microscope (STM6). The discrepancy between the experimental data and the calculated data may arise from fabrication imperfections and environmental factors not taken into account during the simulation.

Figure 11 shows the curve relationship between the displacement and the testing voltage without amplification. As shown in Fig. 11, the experimental data are estimated by the least squares method. After the fitting, the relationship between the displacement of the stage and the testing voltage can be, respectively, expressed as

$$\begin{aligned} y &= -0.00177x + 0.37519, \quad \text{in } +x \text{ direction} \\ y &= +0.00117x + 0.23696, \quad \text{in } +y \text{ direction} \end{aligned} \tag{12}$$

The sensitivity of the piezoresistive sensor is 1.77mV/μm in the *x*-direction and 1.17mV/μm in the *y*-direction. The linearity is 0.814% in the *x*-direction and 0.429% in the *y*-direction.

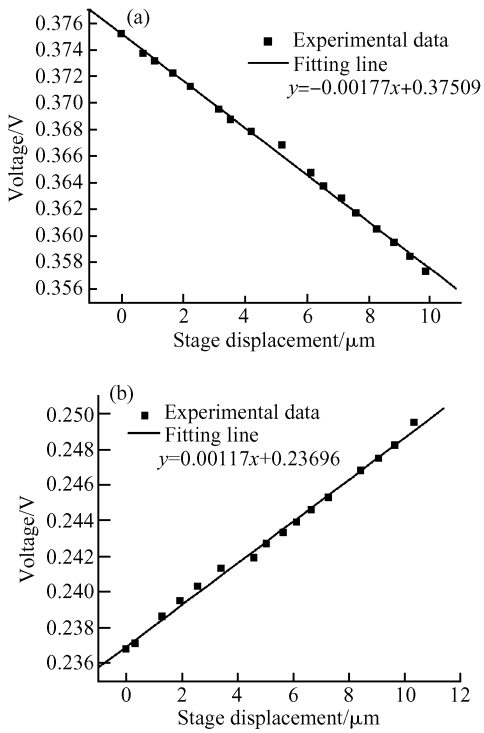

Fig. 11　Relationship between displacement and testing voltage (a) *x* direction; (b) *y* direction

Figure 12 is a bode plot from the spectrum analyzer (HP 4395A). The measured first resonant frequency is found at 983Hz, as shown in Fig. 12. It is 15.9% lower than the simulated first undamped natural frequency, 1169Hz. The discrepancy that is observed may arise from fabrication imperfections since the stiffness of the flexures is sensitive to their dimensions. Furthermore, that approximations made in the finite element modeling and the effect of the damping condition were not taken into account during the simulation all may also contribute to this discrepancy.

6　Conclusion

An integrated micro nano-positioning *xy*-stage for application in nano-operation is designed and fabricated. It is mainly composed of a silicon-based *xy*-stage, comb actuator, and micro displacement sensor based on a vertical sidewall surface piezoresistor. A novel vertical sidewall surface piezoresistor technique based on bulk-micromachining technologies is proposed. Due to the process's high-yield low-cost fabrication technology, the piezoresistor of random dimensions can be located on the vertical sidewall surface easily. The experimental results verify the vertical sidewall surface piezoresistor technique. The sensitivity of the fabricated piezoresistive sensors is better than 1.17mV/μm and the linearity is better than 0.814%. With a driving voltage of 30V, a $\pm 10\mu$m single-axis displacement is measured with a smooth transition between the small and the large actuating regions without crosstalk observed within the resolution of the observations and the first resonance is measured at 983Hz.

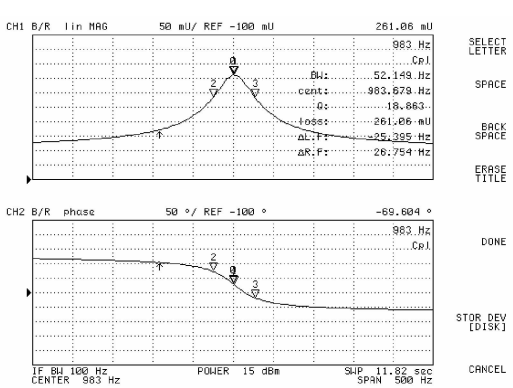

Fig. 12　Measured frequency response of the in-plane component, both amplitude (upper traces) and phases (lower traces) Response curves yielded values of $f_0 = 983$Hz, $Q = 18.86$.

References

[1] Tang W C, Nguyen T H, Howe R T. Laterally driven polysilicon resonant microstructures. Sensors Actuators, 1989, 20: 25

[2] Dong J Y, Mukhopadhyay D, Placid M F. Design, fabrication and testing of a silicon-on-insulator (SOI) MEMS parallel kinematics *XY* stage. J Micromech Microeng, 2007, 17: 1154

[3] Takahashi K, Kwon H N, Saruta K, et al. A two-dimensional *f*-θ micro optical lens scanner with electrostatic comb-drive *XY*-stage. IEICE Electron Express, 2005, 2: 542

[4] Kazuhiro T, Makoto M, Hiroyuki F, et al. A high fill-factor comb-driven *XY*-stage with topological layer switch architecture. IEICE Electron Express, 2006, 3: 197

[5] Ra H, Taguchi Y, Lee D, et al. Two-dimensional MEMS scanner for dual-axis confocal in vivo microscopy. Proc IEEE Micro Electro Mechanical Systems (MEMS), 2005: 862

[6] Sasaki M, Bono F, Hane K. *XY*-stage for scanning media for optical data storage. Proc IEEE Optical MEMS and Their Applications, 2006: 36

[7] Kim C H, Jeong H M, Jeon J U, et al. Silicon micro *xy*-stage with a large area shuttle and no-etching holes for SPM-based data storage. J Microelelctrmechan Syst, 2003, 12: 470

[8] Ando Y. Development of three-dimensional electrostatic stages for scanning probe microscope. Sensors and Acutators A, 2004, 114: 285

[9] Indermuhle P F, Linder C, Brugger J, et al. Design and fabrication of an overhanging *xy*-microactuator with integrated tip for scanning surface profiling. Sensors and Acutators, 1994, 43: 285

[10] Kim C H, Kim Y K. Micro *XY*-stage using silicon on a glass substrate. J Micromech Microeng, 2002, 12: 103

[11] Indermuhle P F, Jaecklin V P, Brugger J, et al. AFM imaging with an *xy*-micropositioner with integrated tip. Sensors Actuators A, 1995, 46/47: 562

[12] Yao J J, Arney S C, MacDonald N C. Fabrication of high frequency two-dimensional nanoactuators for scanned probe devices. J Microelectromech Syst, 1992, 1: 14

[13] Gu L, Li X X, Bao H F, et al. Single-wafer-processed nano-positioning *XY*-stages with trench-sidewall micromachining technonogy. J Micromech Microeng, 2006, 16: 1349

[14] Legtenberg R, Groeneveld A W, Elwenspoek M. Comb-drive actu-

ators for large displacements. J Micromech Microeng, 1996, 6: 320
[15] Bao M H. Micro mechanical transducers: pressure sensors, accelerometers and gyroscopes. NewYork: Elsevier, 2000

用于纳米操作的硅基集成式微型 *xy* 定位平台*

王家畴[1,†] 荣伟彬[1] 孙立宁[1] 李欣昕[2]

(1 哈尔滨工业大学先进机器人与系统国家重点实验室，黑龙江 150001)
(2 中国科学院上海微系统与信息技术研究所 传感技术国家重点联合实验室，上海 200050)

摘要：针对纳米级定位平台小型化和高定位精度的要求，基于体硅工艺研制出一种集结构、驱动和位移检测一体化的集成式微型纳米级 *xy* 定位平台. 采用体硅双面深度反应离子刻蚀(DRIE)技术释放出高深宽比的静电梳齿驱动器、检测梁及定位平台结构. 由于定位平台属于面内运动，为了提高面内运动位移检测的灵敏度提出了一种利用离子注入工艺和 DRIE 技术相结合制作检测梁侧壁压阻的方法，并利用该侧壁压阻工艺成功地把基于侧壁压阻式的位移传感器集成到微型 *xy* 定位平台上. 实验测试表明，位移传感器的灵敏度优于 1.17mV/μm，线形度优于 0.814%，当驱动电压取 30V 时，定位平台的单轴输出位移可达 $\pm 10\mu$m，并且定位平台 *x* 方向和 *y* 方向上的位移耦合量非常小；在空气条件下测得定位平台的一阶固有频率为 983Hz.

关键词：微机电系统；集成式微型 *xy* 定位平台；静电梳齿致动器；面内垂直侧壁表面压阻
PACC：0670D；2940T；2940P
中图分类号：TP212 **文献标识码**：A **文章编号**：0253-4177(2008)10-1932-07

* 国家杰出青年基金(批准号：50725518)，国家高技术研究发展计划(批准号：2007AA04Z315)及长江学者和创新团队发展计划资助项目
† 通信作者. Email: jiatao_wang@163.com
2008-05-12 收到，2008-06-19 定稿